

The force-freeness of the solar photosphere: Revisit with new approach and large datasets

MEI ZHANG^{1,2,3} AND HAOCHENG ZHANG⁴

¹*National Astronomical Observatories, Chinese Academy of Sciences, Beijing 100101, China; zhangmei@nao.cas.cn*

²*School of Astronomy and Space Sciences, University of Chinese Academy of Sciences, Beijing 100049, China*

³*High Altitude Observatory, National Center for Atmospheric Research, 3080 Center Green Drive, Boulder, CO 80301, USA*

⁴*Jericho High School, 99 Cedar Swamp Road, Jericho, NY 11753, USA*

ABSTRACT

Although it is generally believed that the solar photosphere is not magnetically force-free owing to its high plasma β , the estimations of force-freeness using observed magnetograms have produced disputable results. Some studies confirmed that the photosphere is largely not force-free whereas some authors argued that the photosphere is not far away from being force-free. In a previous paper of ours we demonstrated that, due to the fact that the noise levels of the transverse field in the magnetograms are much larger than those of the vertical field, wrong judgements on the force-freeness could be made: a truly force-free field could be judged as being not-force-free and a truly not-force-free field could be judged as being force-free. Here in this letter we propose an approach to overcome this serious problem. By reducing the spatial resolution to lower the noise level, the heavy influence of the measurement noise on the force-freeness judgement can be significantly suppressed. We first use two analytical solutions to show the success and the effectiveness of this approach. Then we apply this new approach to two large datasets of active region magnetograms, obtained with the HMI/SDO and SP/Hinode, respectively. Our analysis shows that the photospheric magnetic fields are actually far away from being force-free. Particularly and most notably, the mean value of F_z/F_p (where F_z the net Lorentz force in the vertical direction and F_p the total Lorentz force) is as low as -0.47 , with more than 98% of the active regions having $|F_z/F_p| > 0.1$, when using the SP/Hinode magnetograms of true field strength.

Keywords: The Sun — Solar Photosphere — Solar Magnetic Fields

1. INTRODUCTION

It is well known that the Sun's magnetic field is the engine and energy source driving all solar phenomena (Charbonneau 2014). These phenomena collectively define the solar activity, including those violent eruptions such as coronal mass ejections (Zhang & Low 2005). An accurate understanding on how the solar magnetic fields are produced and evolved is then very crucial. However, so far only the photospheric magnetic field can be measured with fair accuracy and reasonable spatial and temporal

resolutions. The large bodily coronal magnetic fields are mainly estimated from nonlinear force-free field extrapolations (Wiegelmann & Sakurai 2021).

It is a common practice that the observed photospheric magnetograms are used as the boundary conditions in the force-free field extrapolations. Then as a first step, whether the observed photospheric magnetograms satisfy the force-free condition or not needs to be checked. Gary (2001) pointed out that the solar photosphere has its $\beta > 1$, so it is likely that the photosphere is not force-free.

Low (1985) proposed a method to check whether the observed magnetograms satisfy the force-free condition or not. He pointed out that, in an isolated magnetic structure, a necessary condition for a force-free field to exist above a measured layer is:

$$F_x \ll F_p, F_y \ll F_p, F_z \ll F_p, \quad (1)$$

where F_x , F_y and F_z are the components of the net Lorentz force, and F_p is the characteristic magnitude of the total Lorentz force that can be brought to bear on the atmosphere if the magnetic field is not force-free. These components of net Lorentz force can be estimated, using Low (1985) method from the observed vector magnetograms, by following formula:

$$F_x = -\frac{1}{4\pi} \int B_x B_z dx dy, \quad (2)$$

$$F_y = -\frac{1}{4\pi} \int B_y B_z dx dy, \quad (3)$$

$$F_z = -\frac{1}{8\pi} \int (B_z^2 - B_x^2 - B_y^2) dx dy, \quad (4)$$

$$F_p = \frac{1}{8\pi} \int (B_z^2 + B_x^2 + B_y^2) dx dy, \quad (5)$$

where B_x , B_y and B_z are the three components of the vector magnetic field, in which B_z is the vertical magnetic field and B_x , B_y are the two components of the horizontal magnetic field B_t .

Metcalf et al. (1995) presents the first study of using Low (1985) method to estimate the force-freeness of an active region NOAA 7216. It is also the first study where a value of $|F_x/F_p|$, $|F_y/F_p|$ and $|F_z/F_p|$ being less than 0.1 is suggested, as the criteria for a measured magnetic field being considered as being force-free. This criteria has been adopted and used by the community in all afterwards studies as well as in ours.

By studying the spectropolarimeter data from Mees Solar Observatory using the Na I $\lambda 5896$ spectral line, Metcalf et al. (1995) concluded that NOAA 7216 is not force-free in the photosphere but becomes force-free at a height of about 400 km and above in the chromosphere. However, also using the Mees spectropolarimeter data but on the Fe 6301.5/6302.5 lines, Moon et al. (2002) analyzed 12 vector magnetograms of three flare-eruptive active regions and concluded that the photospheric magnetic fields are not far away from being force-free. The median value of $|F_z/F_p|$ that Moon et al. (2002) found is 0.13, which is far smaller than the value (around 0.5) that Metcalf et al. (1995) obtained for the photospheric magnetic field. Tiwari (2012) studied a few high spatial resolution SP/Hinode magnetograms, and also concluded that the sunspot magnetic fields are not far away from being force-free, although their force-freeness may change with the time.

Disputable results continue to appear. [Liu et al. \(2013\)](#) carried out a statistical study by analyzing a sample of 925 magnetograms which were taken with the filter-based Solar Magnetic Field Telescope (SMFT) of the Huairou Solar Observing Station (HSOS). They found that only about 25% of the magnetograms can be considered as close to be force-free, i.e., most (75%) of the photospheric magnetic fields are not force-free. Yet when [Duan et al. \(2020\)](#) studied a sample of 3536 HMI/SDO magnetograms of 51 flux emerging active regions, they concluded that the emerging active regions are “very close to a force-free state, which is not consistent with theories as well as idealized simulations of flux emergence”.

Different from above studies that directly applied Equations (2)-(5) to observed magnetograms and gave their respective conclusions, [Zhang et al. \(2017\)](#) tried to reconcile the differences in the results of previous studies by carrying out a systematic study on how the instrumental effects could influence the judgement of the force-freeness. They studied how the limited field of view, the instrument sensitivity and the measurement noise could affect the force-freeness judgement. They found that as long as the flux balance condition is roughly satisfied, the influences of the field of view and the instrument sensitivity on the force-freeness judgement are not large. However, the influence of the measurement noise on the force-freeness judgement is huge. It could make a truly force-free field be wrongly judged as being not-force-free and a truly not-force-free field be wrongly judged as being force-free. This is due to the fact that the noise level of the transverse field is about or even more than ten times of that of the vertical field in the magnetograms ([Wiegelmann et al. 2012](#); [Hoeksema et al. 2014](#)). The square of the noises of the transverse fields could not cancel out those of the vertical fields when using Equation (4), a point discussed in detail in the discussion section of [Zhang et al. \(2017\)](#). They also pointed out that cutting the magnetograms at a high signal-to-noise level would help some but cannot overturn the result. Their examples show that even when cutting the magnetograms at a 2σ level (which is the case in most studies), the noises in the remaining 10% data points can still affect the force-freeness judgement.

The study of [Zhang et al. \(2017\)](#) may explain why previous studies gave disputable results. It may merely depend on how the authors have handled the measurement noises. In other words, the measurement noises may have influenced the force-freeness judgments in a way that has been largely underestimated in most studies. In this paper, we propose an approach to overcome this problem: by reducing the spatial resolution to lower the noise level. In doing so, the heavy influence of the measurement noise on the force-freeness judgement will be significantly suppressed. We first use two analytical magnetic field solutions, in Section 2, to show the success and the effectiveness of this approach. Then we apply this approach to two large datasets of active region magnetograms. The data and the samples will be described in Section 3. The analysis and results will be presented in Section 4. A brief summary and discussion will be given in Section 5.

2. THE MODEL

In this section we use two analytical solutions, one known force-free magnetic field, described in [Low & Lou \(1990\)](#), and one known force-balanced non-force-free magnetic field, described in [Low \(1992\)](#), to show the effectiveness of our proposed approach: reducing the spatial resolution to lower the noise level so that the heavy influence of the measurement noise on the force-freeness judgement could be significantly suppressed. Similar approach has been proposed and tested in [Jiang & Zhang \(2018\)](#). For the completion of this paper, we present it here using two different solutions from theirs.

The top two panels of Figure 1 show the two vector magnetic fields we used. The one in the left top panel is constructed using nonlinear force-free solutions described in [Low & Lou \(1990\)](#). It is the same to the one presented in the Figure 4 of [Low & Lou \(1990\)](#), generated by $P_{1,1}$ with $l = 0.3$ and $\Phi = \pi/4$. Red contours outline the positive vertical magnetic fields ($B_z > 0$) and the blue lines outline the negative vertical magnetic fields ($B_z < 0$). The green lines show where the $B_z = 0$ lies. The arrows in the plane show the directions of the transverse fields (\mathbf{B}_t), with their lengths in proportion to the magnitudes of the transverse field ($|\mathbf{B}_t|$).

The constructed magnetogram has a size of 1024×1024 pixels². Following [Zhang et al. \(2017\)](#), we have rescaled the vector magnetogram to make its maximum strength of B_z to be 2000 G. This makes the field strengths in the obtained magnetogram more close to the observed ones. Specifically, a factor of 6.80983 has been multiplied to B_x , B_y and B_z , making the minimum of B_z changing from its original -293.693 G value in [Low & Lou \(1990\)](#) solution to -2000 G. Using Equations (2)-(5), we get $F_x/F_p = -0.000039$, $F_y/F_p = 0.000649$ and $F_z/F_p = -0.002797$, verifying its nature as being force-free.

In order to use Equations (2)-(5) to estimate the force-freeness, the magnetogram needs to have its positive and negative fluxes roughly balanced. The quantity, flux imbalance (MI), defined as

$$MI = \frac{|F^+ - F^-|}{F^+ + F^-} \times 100\% \quad , \quad (6)$$

where F^+ and F^- are upward ($B_z > 0$) and downward ($B_z < 0$) magnetic fluxes respectively, is usually estimated and used as the indicator of the degree of flux balance. Most previous studies use a criteria of 10%, that is, magnetogram whose magnetic imbalance (MI) is within 10% is regarded as satisfying the prerequisite for applying the [Low \(1985\)](#) method. Our previous study ([Zhang et al. 2017](#)) has also verified the applicability of this criteria. The MI value of this [Low & Lou \(1990\)](#) solution field is -3.09% .

Presented in a similar way in the right top panel of Figure 1 is a vector magnetic field constructed using the magnetostatic solutions described in [Low \(1992\)](#). The vertical magnetic field (B_z) is obtained using model parameters listed in the Table 1 of [Low \(1992\)](#), making the B_z similar to that presented in the Figure 1 of [Low \(1992\)](#), except that the field of view has been shifted a little bit up in the y-direction in order to make the obtained field possessing a value of MI less than 10%. For other model parameters in [Low \(1992\)](#), we use $\alpha_0 = 0.3$ and $a = 0.5$. Similarly, the constructed vector magnetogram has a size of 1024×1024 pixels² and has been rescaled to make its maximum strength of B_z to be 2000 G. This field has $F_x/F_p = 0.002630$, $F_y/F_p = -0.020666$ and $F_z/F_p = -0.144740$. So, by its F_z/F_p value, it is a non-force-free field. Its MI is 0.635%.

The remaining six panels of Figure 1 show how reducing the spatial resolution could influence the force-freeness judgement. The left panels are of the [Low & Lou \(1990\)](#) force-free field, and the right panels are of the [Low \(1992\)](#) non-force-free field. The x-axis is the resolution-index R , where $R = 0$ means that the original spatial resolution (magnetograms of 1024×1024 pixels²) is used to calculate the F_x/F_p , F_y/F_p and F_z/F_p . $R = 1$ means that the original 1024×1024 pixels² magnetograms have been ‘‘rebinning’’ (using IDL program) to 512×512 pixels² magnetograms to calculate the F_x/F_p , F_y/F_p and F_z/F_p . Similarly, $R = 2, 3, 4$ means that the magnetograms have been further rebinned to 256×256 pixels², 128×128 pixels² and 64×64 pixels² magnetograms, respectively, to calculate the F_x/F_p , F_y/F_p and F_z/F_p . In short, from $R = 0$ to $R = 4$, in each step, the spatial resolution of the magnetograms is reduced to 1/2 of the previous ones, and the spatial resolution in $R = 4$

magnetograms is only 1/16 of the original ones. Similar practice is done for all reducing spatial resolution processes in the later development of the paper.

We can see from these six panels of Figure 1 that, even though the spatial resolutions of the magnetograms have been greatly reduced, the values of F_x/F_p , F_y/F_p and F_z/F_p do not change much. Take the bottom left panel for example, the F_z/F_p values change from -0.002797 in the $R = 0$ magnetogram to -0.002594 in the $R = 4$ magnetogram, keeping correctly “judging” that the studied magnetic field is force-free. Similarly, in the bottom right panel, F_z/F_p values change from -0.144740 in the $R = 0$ to -0.144711 in the $R = 4$, keeping correctly “judging” that the studied magnetic field is not force-free. This is understandable, because the formula we use to calculate the F_x , F_y and F_z are all integrals on the whole field of view. Reducing the spatial resolution will certainly change the field magnitude in each data point, but the changes in the integrals may not be that large, particularly what we calculated are their ratios to F_p .

Note that above analysis are all done on the analytical solution fields which have no measurement noises. In reality, the used magnetograms, inverted from polarization measurements, all possess measurement noises. In particular, the noise level of the transverse field is about ten times of that of the vertical field in the magnetograms (Wiegmann et al. 2012; Hoeksema et al. 2014). This will bring in serious problem as discussed in Zhang et al. (2017). In Figure 2 we present this influence again and in particular we show how reducing the spatial resolution to lower the noise level could significantly reduce this bad influence of the measurement noise on the force-freeness judgement.

Similar to Figure 1, the left panels in Figure 2 present the F_x/F_p , F_y/F_p and F_z/F_p values of the Low & Lou (1990) force-free field and the right panels are for the Low (1992) non-force-free field. Following Zhang et al. (2017), to mimic the effect of the measurement noise in the observed magnetogram, we have added a white noise to each component of the vector magnetogram. That is, the B_x , B_y and B_z component in the above two 1024×1024 pixels² magnetograms are replaced by $B_x + \sigma_x$, $B_y + \sigma_y$ and $B_z + \sigma_z$, respectively, where σ_x , σ_y and σ_z are the white noise of each field component. σ_z in each data point is created by multiplying σ_z^0 with a normally-distributed random number, similarly σ_x and σ_y by multiplying σ_x^0 and σ_y^0 with a normally-distributed random number of their own. Also following Zhang et al. (2017), to imitate the real magnetograms, we have assumed σ_x^0 and $\sigma_y^0 = 10 \sigma_z^0$, with σ_z^0 increasing from $0 G$ to $24 G$ with a constant step of $1 G$. The values of σ_z^0 are plotted as the x-axis in Figure 2.

The black lines in Figure 2 show the results of F_x/F_p (top panels), F_y/F_p (middle panels) and F_z/F_p (bottom panels) using above 1024×1024 pixels² noise-bearing magnetograms. We can see that, similar to what found in Zhang et al. (2017), the measurement noises give little influence to F_x/F_p and F_y/F_p . The variations of F_x/F_p and F_y/F_p , with different noise levels, are all very minor. However, the F_z/F_p increases monotonously with the increase of the noise level. When σ_z^0 is larger than $9 G$ ($90 G$ for σ_x^0 and σ_y^0), the F_z/F_p in the left bottom panel has increased to a value larger than 0.1 . This means that, at this noise level and above, this real force-free magnetic field could be wrongly judged as being not-force-free. Similarly, When σ_z^0 is larger than $14 G$ ($140 G$ for σ_x^0 and σ_y^0), the F_z/F_p in the right bottom panel has increased to a value larger than -0.1 . This means that, at this noise level and above, this real non-force-free magnetic field could be wrongly judged as being force-free.

This serious problem will be significantly alleviated if we reduce the spatial resolutions of the magnetograms. In Figure 2, the blue lines show the F_x/F_p , F_y/F_p and F_z/F_p values for the $R = 1$

magnetograms, where the noise-bearing 1024×1024 pixels² magnetograms have been rebinned to 512×512 pixels² magnetograms. We can see from the bottom left panel of Figure 2, now σ_z^0 needs to be as large as 17 G to make a wrong judgement. And from the bottom right panel of Figure 2, we see that no wrong judgement will be made now, even though the F_z/F_p values still monotonously increase with the noise level. If we further decrease the spatial resolutions, the influences of the noise level on the force-free judgement will become less and less. This is evident in the red, green and yellow lines, which show the F_x/F_p , F_y/F_p and F_z/F_p values for the $R = 2$, $R = 3$ and $R = 4$ magnetograms, respectively. We can see that, when $R = 4$ is applied, the influence of the measurement noise has become almost neglectable. The two yellow lines in the bottom panels of Figure 2 have become almost horizontal. This means that when $R = 4$ is applied, the estimated F_x/F_p , F_y/F_p and F_z/F_p values from the noise-bearing magnetograms have become nearly the same to their true values, independent of the noise level. This proves that reducing the spatial resolution can significantly suppress the bad influence of the measurement noise.

Before we apply this method to two large datasets in the following sections of this paper, two notes are in order here. First, the analytic models we used here do not have small-scale structures as those in real data. With real data, the smoothing would change the basic magnetic-field structure in a larger degree. However, this will not change any conclusions presented in this section. This can be seen from the two examples in Jiang & Zhang (2018). The two model fields there, reconstructed from observed magnetograms, do have small-scale structures. And similar analysis as those done in this section gives the same conclusion. An English version of Jiang & Zhang (2018) can be found in Jiang & Mei (2019). Secondly, we need to point out that our noise model, which fixes the ratio between the noise of the transverse field and that of the vertical field as a number of 10, is probably over-simplified. The real noise levels in magnetograms may vary from one to another and may also vary between data points and dependent on the field strength even within one magnetogram. Quoting from Wiegmann et al. (2012) that “the random errors in the line-of-sight component are about 5 G, while the uncertainty in the transverse field is as much as 200 G in weak field regions and as little as 70 G where the field is strong”, our approach of fixing the ratio as a number of 10 is indeed simple and somewhat conservative. However, in our regard, more accurate and more complicated noise models will not change our results in any qualitative way, if not even strengthen our conclusion further.

3. THE DATA AND SAMPLES

We construct two large datasets, one from HMI/SDO observations and one from SP/Hinode observations.

The first dataset uses the vector magnetograms taken by Helioseismic and Magnetic Imager (HMI)/SDO (Scherrer et al. 2012). HMI/SDO observes the full solar disk at FeI $\lambda 6173$ with a 4096×4096 CCD detector to study the oscillations and the magnetic fields on the solar photosphere. The spatial resolution is $0.91''$ with a $0.5''$ pixel size. A Milne–Eddington based inversion code (Borrero et al. 2011) is used to derive the vector magnetograms from the filtergrams taken at six wavelength positions. The azimuthal 180° ambiguity was resolved by the “minimum energy” algorithm (Metcalf et al. 2006).

We use the hmi.sharp_cea_720s series of the active-region vector magnetograms (Bobra et al. 2014). In this series of the data, the disambiguated vector magnetograms are deprojected using Lambert cylindrical equal area projection method, presented as (B_r, B_θ, B_ϕ) in heliocentric spherical coor-

ordinates which corresponds to $(B_z, -B_y, B_x)$ in heliographic coordinates. Each region in this series is given a HARP number. From May 2010 to April 2020, the HARP number increases from $HARPNUM = 1$ to $HARPNUM = 7412$. For each HARPNUM during this period, we download the one whose longitude is closest to the central meridian. We end up with 3838 vector magnetograms downloaded. Among these 3838 magnetograms we further select those having a NOAA number assigned in the fits header (by the “noaa_ar” keyword in the header). This reduces the number of selected magnetograms to be 1335. Finally, we only use those magnetograms whose MI is less than 10%. This results in a sample of 547 HMI/SDO vector magnetograms. In these 547 magnetograms, the largest one has a field of view of $1715'' \times 452''$, the smallest field of view is $108'' \times 84''$. The median value of the field of view is around 62200 arcsec^2 , roughly equivalent to $600 \times 410 \text{ pixels}^2$ with $0.5''/\text{pixel}$.

The second dataset uses the vector magnetograms obtained by the Spectro-polarimeter (SP) aboard Hinode (Kosugi et al. 2007). Using a $0.16'' \times 164''$ slit, SP/Hinode obtains line profiles of two magnetically sensitive Fe lines at 630.15 and 630.25 nm and nearby continuum. The resolution of these magnetograms is about $0.32''/\text{pixel}$ for the fast maps we used. The SP/Hinode data are calibrated (Lites & Ichimoto 2013) and inverted at the Community Spectro-polarimetric Analysis Center (CSAC, <http://www.csac.hao.ucar.edu/>). The inversion is based on the assumption of the Milne-Eddington atmosphere model and a nonlinear least-square fitting technique where the analytical Stokes profiles are fitted to the observed profiles. The inversion gives 36 parameters including the three components of magnetic field and the filling factor. The 180° azimuth ambiguity is resolved by setting the directions of the transverse fields most closely to a current-free field.

We searched the CSAC webpage and downloaded 448 magnetograms for active regions observed by the SP/Hinode from January 2006 to October 2019. Each of these 448 magnetograms is of one active region and is the one that is closest to the central meridian among all those observations of this active region. Two samples are constructed from these 448 magnetograms, depending on whether the “true field strength” or the “flux density” magnetograms are used. The “true field strength” magnetograms use the inversion-derived field strength B , field inclination γ and field azimuth ϕ to get $B_x = B \sin(\gamma) \cos(\phi)$, $B_y = B \sin(\gamma) \sin(\phi)$ and $B_z = B \cos(\gamma)$. In the “flux density” magnetograms, $B_x = \sqrt{f} \cdot B \sin(\gamma) \cos(\phi)$, $B_y = \sqrt{f} \cdot B \sin(\gamma) \sin(\phi)$ and $B_z = f \cdot B \cos(\gamma)$, where f is the filling factor. Following the hmi.sharp_cea_720s series procedure, these vector magnetic fields are transformed to local heliographic coordinates. Then as before, only those magnetograms with MI less than 10% are used. This makes our SP/Hinode “flux density” sample contain 144 magnetograms and the SP/Hinode “true field strength” sample contain 138 magnetograms. The reason that these two samples are of a different size is that, when calculating the MI value of each magnetogram, we have used their respective B_x , B_y and B_z in either the “flux density” magnetogram or the “true field strength” magnetogram.

4. ANALYSIS AND RESULTS

In this section we present our analysis and results on the three samples we constructed: the HMI/SDO sample of 547 active regions, the SP/Hinode “flux density” sample of 144 active regions and the SP/Hinode “true field strength” sample of 138 active regions.

For each magnetogram in each sample, we first calculate their F_x/F_p , F_y/F_p and F_z/F_p values with the original spatial resolution (the $R = 0$ magnetograms). Then, we decrease the spatial resolution of each magnetogram to 1/2 of its original one and calculate the F_x/F_p , F_y/F_p and F_z/F_p values again

but using these $R = 1$ magnetograms. Same procedure is done for the $R = 2$, $R = 3$ and $R = 4$ magnetograms. That is, for each magnetogram in the samples, we have calculated the F_x/F_p , F_y/F_p and F_z/F_p values five times, with the magnetogram rebinned to lower and lower spatial resolutions, from $R = 0$ (original spatial resolution) to $R = 4$ (1/16 of the original spatial resolution). Note that we have not done any “cutting” of the data points, that is, we did not remove the data points with low signal-to-noise ratios as most other researches do. This is because the results in the previous section have shown that reducing spatial resolution is a very efficient way to suppress the influence of measurement noise. Also, as mentioned before, Zhang et al. (2017) has showed that “cutting” is not a very efficient method and cannot fully remove the bad influence of the measurement noise.

Figure 3 shows how the F_x/F_p , F_y/F_p and F_z/F_p values change with the spatial resolution. Here NOAA 11739 is selected as an example because it is a common active region in all three samples. The top panels of Figure 3 show the magnetograms of this active region, left panel of HMI/SDO data, middle panel of the SP/Hinode “flux density” magnetogram and the right panel of the SP/Hinode “true field strength” magnetogram. We can see that the field of view of HMI/SDO magnetogram is somewhat different from that of the SP/Hinode magnetograms. That is because we have not done anything to change the HMI/SDO HARP field of view, neither to SP/Hinode field of view. So in our three samples, although there are many common active regions, the sizes of their field of views are usually different, between the HMI/SDO magnetograms and the SP/Hinode ones.

The F_x/F_p , F_y/F_p and F_z/F_p values of this active region are plotted as green filled-diamonds in the remaining panels of Figure 3, linked by a purple line in each panel. Again, left panels are of the HMI/SDO magnetogram, middle panels of the SP/Hinode “flux density” magnetogram and the right panels of the SP/Hinode “true field strength” magnetogram. As those in Figure 1, the x-axis is the resolution-index R . We can see that, with the increase of R (decrease of spatial resolution), the F_x/F_p and F_y/F_p values do not change much, for all three magnetograms. This is consistent with what we found in previous section, as shown in Figure 2.

However, from the bottom three panels of Figure 3 we can see that, the F_z/F_p values decrease significantly with the increase of R . For the HMI/SDO magnetogram, the F_z/F_p values change from 0.046 at the $R = 0$ to -0.25 at the $R = 4$. This means that, we could wrongly judge this field as being force-free if we use the $R = 0$ magnetogram, while it is actually not force-free from its $F_z/F_p = -0.25$ value using the $R = 4$ magnetogram. Similarly, for the SP/Hinode “flux density” magnetogram, the F_z/F_p values change from -0.34 at the $R = 0$ to -0.38 at the $R = 4$. Its $F_z/F_p < -0.1$ property confirms that this field is not force-free. The relatively small variation of F_z/F_p values with the R indicates that the noise level in the SP/Hinode magnetograms are not large, particularly compared to those in the HMI/SDO magnetograms. Another advantage of the SP/Hinode observations is that it can give us the true field strength of the magnetic field rather than just the flux density. From the right bottom panel of Figure 3, we can see that the F_z/F_p values change from -0.54 at the $R = 0$ to -0.61 at the $R = 4$, which means that the magnetic field of this active region is actually far away from being force-free.

Figure 4 shows the histograms of the F_x/F_p (left panels), F_y/F_p (middle panels) and F_z/F_p (right panels) values of the 547 HMI/SDO magnetograms. Shown from top to bottom panels are the histograms of these values obtained from the $R = 0$, $R = 1$, $R = 2$, $R = 3$ and $R = 4$ magnetograms, respectively. The blue histograms are of the active regions in the northern hemisphere and the green ones of the active regions in the southern hemisphere. The mean values of F_x/F_p or F_y/F_p or F_z/F_p

are calculated, shown by the vertical purple line in each panel with the number listed in the top corner of each panel. Also listed in each panel is the non-force-freeness number (NF), which shows the percentage of the active regions that have their $|F_x/F_p| > 0.1$ in left panels or their $|F_y/F_p| > 0.1$ in middle panels or their $|F_z/F_p| > 0.1$ in right panels.

We can see that the mean values of F_x/F_p and F_y/F_p are all small, and do not change much with the increase of R . However, the mean values of F_z/F_p decrease from -0.021 in the $R = 0$ panel to -0.210 in the $R = 4$ panel, a tendency same to that of the NOAA 11739 in Figure 3. Here we see again that the active regions could be judged as being force-free by their $|F_z/F_p|$ values in the $R = 0$ magnetograms whereas they are actually not force-free when judging from the $R = 4$ magnetograms. These mean values are also plotted in the left panels of Figure 3 as the blue filled-circles linked by red lines.

From the right panels of Figure 3 we can also see that, although the mean values of F_z/F_p decrease from -0.021 in the $R = 0$ panel to -0.210 in the $R = 4$ panel, the distributions of the histograms do not change much. Note that in previous studies (Moon et al. 2002; Tiwari 2012; Duan et al. 2020) where the authors claimed that their data are nearly force-free, some of their $|F_z/F_p|$ show values larger than 0.1. So in terms of the distribution of histograms, our results do not differ very much from most of the previous publications. It is the systematic shift of the whole distribution with the increase of R shows the effect of reducing measurement noises.

From Figure 4, we can see that, even though both the mean values of F_x/F_p and F_y/F_p are small, they actually have very different distributions. Most active regions have their $|F_x/F_p| < 0.1$. This can be seen from the relatively small values of NF (from 7.9% to 15.0%) listed in each of the left panels. However, for the F_y/F_p values, even though their mean values are small (from -0.007 to -0.010), most active regions actually have their $|F_y/F_p|$ values larger than 0.1. This can be seen from that their NF numbers lie between 75.7% to 78.4%. The NF numbers of F_z/F_p increase from 41.9% in the $R = 0$ panel to 75.1% in the $R = 4$ panel. When accounting for all three components of the net Lorentz force, only about 14% of these HMI/SDO magnetograms have their $|F_x/F_p| < 0.1$, $|F_y/F_p| < 0.1$ and $|F_z/F_p| < 0.1$.

From Figure 4 we can also see that, there is a north-south asymmetric in the F_y/F_p distributions. F_y/F_p tends to be negative for active regions in the northern hemisphere and positive in the southern hemisphere. We will see this north-south asymmetry also exists in the F_y/F_p values of the SP/Hinode “flux density” magnetograms (Figure 5), but becomes less evident in the SP/Hinode “true field strength” magnetograms (Figure 6). The reasons for this north-south asymmetry as well as for the difference between using the “flux density” magnetograms and the “true field strength” magnetograms are not known. This north-south asymmetry implies an existence of a net equator-ward force. A simple guess is that it is there to act against the meridional flow that drives the regions in the opposite hemispheres apart to the poles. To our knowledge, such an asymmetry has not been reported before. It deserves further studies to check and analyze.

Similar to Figure 4, Figure 5 shows the histograms of the F_x/F_p , F_y/F_p and F_z/F_p values, but for the 144 SP/Hinode “flux density” magnetograms. We see that the mean values of F_x/F_p and F_y/F_p are also very small, and also do not change much with the increase of R . The mean values of F_z/F_p decrease from -0.274 in the $R = 0$ panel to -0.328 in the $R = 4$ panel, the same tendency as those in Figures 3 and 4. We also see that the NF values of F_x/F_p are relatively small (from 6.3% to 8.3%), are large for F_y/F_p (from 59.7% to 63.2%), and become even larger for F_z/F_p (from 90.3% to 91.7%).

When accounting for all three components of the net Lorentz force, none of these SP/Hinode “flux density” magnetograms have their $|F_x/F_p| < 0.1$, $|F_y/F_p| < 0.1$ and $|F_z/F_p| < 0.1$.

Similarly, Figure 6 shows the histograms of the F_x/F_p , F_y/F_p and F_z/F_p values, but for the 138 SP/Hinode “true field strength” magnetograms. Again we see that the mean values of F_x/F_p and F_y/F_p are small, and also do not change much with the increase of R . The mean values of F_z/F_p decrease from -0.406 in the $R = 0$ panel to -0.471 in the $R = 4$ panel, the same tendency as those in Figures 3, 4 and 5. We also see here that the NF values of F_x/F_p are relatively small (from 9.4% to 11.6%), are large for F_y/F_p (from 68.1% to 71.0%), and become even larger for F_z/F_p (from 97.1% to 98.6%). Again, when accounting for all three components of net Lorentz force, none of these SP/Hinode “true field strength” magnetograms have their $|F_x/F_p| < 0.1$, $|F_y/F_p| < 0.1$ and $|F_z/F_p| < 0.1$. Most notably here is that, the mean values of F_z/F_p are all smaller than -0.4 . The mean value of F_z/F_p for the $R = 4$ magnetograms becomes as low as -0.471 , a number that is very close to what [Metcalf et al. \(1995\)](#) found in their study.

5. SUMMARY AND DISCUSSION

In a previous study ([Zhang et al. 2017](#)) it was pointed out that, the much larger noise level of the transverse field in the observed magnetograms could bring in serious problem in the force-freeness judgement. It could make a truly force-free field be wrongly judged as being non-force-free and could also make a truly non-force-free field be wrongly judged as being force-free.

In this paper we have proposed an approach to overcome this serious influence of the measurement noise. We proposed to reduce the spatial resolution of the magnetograms to lower the noise level so that the serious influence of the measurement noise on the force-freeness judgement could be significantly suppressed. Using two analytical magnetic fields, one being force-free and one being non-force-free, we have shown that our proposed approach is very effective. The bad influence of the measurement noise could be largely removed when reducing the spatial resolution of the magnetograms to 1/16 of the original ones.

We then applied this approach to three samples, constructed from two datasets of the HMI/SDO active region magnetograms and the SP/Hinode active region magnetograms, respectively. Our analysis has shown that all three samples give consistent results that the photospheric magnetic field is not force-free. Most, if not all, active regions have one of their $|F_x/F_p|$ or $|F_y/F_p|$ or $|F_z/F_p|$ greater than 0.1. In particular, the mean value of F_z/F_p is as low as -0.47 when using the SP/Hinode “true field strength” magnetograms, a value very close to what firstly found in [Metcalf et al. \(1995\)](#) for the photospheric magnetic field.

It is worthy of mentioning here that the non-force-freeness of the photospheric magnetic field does not exclude the applicability of using observed photospheric magnetograms as the boundary conditions for nonlinear force-free field extrapolations. Not only because the photospheric vector magnetograms are only those currently we can get with fair accuracy and reasonable spatial and temporal resolutions, but also because up-to-date extrapolation methods have taken into account this non-force-freeness fact by modifying the observed magnetograms to be force-free ([Wiegmann et al. 2006](#); [Wiegmann & Inhester 2010](#); [Wiegmann et al. 2012](#)). These modified magnetograms should be regarded as presenting the chromospheric magnetic fields rather than the photospheric ones.

At the same time, “many nonlinear force-free coronal-field extrapolations based directly on the photospheric vector magnetograms generally agrees with each other to some extent” ([Duan et al. 2020](#)) cannot be used as a proof that the photospheric magnetic field is close to be force-free. However,

using the observed force-freeness to test and constrain flux emergence models and simulations is indeed a very interesting practice. Our preliminary study shows that, except for the very early stage of the flux emergence, the emerged active region quickly settles to $F_z/F_p < -0.1$, rather than the large positive F_z/F_p values shown in Toriumi & Takasao (2017) and Toriumi et al. (2020). The point that an inconsistency exists between the observation and the simulation has already been touched by Duan et al. (2020). It certainly warrants a future detailed study on the evolution of the force-freeness in emerging active regions, using the method carried out in this paper, to test the consistency between the observation and various flux emergence simulations.

We thank the anonymous referee for helpful comments and suggestions that improved the presentation of this paper. The HMI data used in this paper were provided by courtesy of NASA/SDO and the HMI science team. Hinode is a Japanese mission developed and launched by ISAS/JAXA, collaborating with NAOJ as a domestic partner, NASA and STFC (UK) as international partners. The Hinode SOT/SP data used in this paper were distributed by the Community Spectropolarimetric Analysis Center of HAO/NCAR. This work is supported by the National Natural Science Foundation of China (grant No. 11973056) and the National Key R&D Program of China (grant No. 2021YFA1600500).

REFERENCES

- Bobra, M. G., Sun, X., Hoeksema, J. T., et al. 2014, *SoPh*, 289, 3549, doi: [10.1007/s11207-014-0529-3](https://doi.org/10.1007/s11207-014-0529-3)
- Borrero, J. M., Tomczyk, S., Kubo, M., et al. 2011, *SoPh*, 273, 267, doi: [10.1007/s11207-010-9515-6](https://doi.org/10.1007/s11207-010-9515-6)
- Charbonneau, P. 2014, *ARA&A*, 52, 251, doi: [10.1146/annurev-astro-081913-040012](https://doi.org/10.1146/annurev-astro-081913-040012)
- Duan, A., Jiang, C., Toriumi, S., & Syntelis, P. 2020, *ApJL*, 896, L9, doi: [10.3847/2041-8213/ab961e](https://doi.org/10.3847/2041-8213/ab961e)
- Gary, G. A. 2001, *SoPh*, 203, 71, doi: [10.1023/A:1012722021820](https://doi.org/10.1023/A:1012722021820)
- Hoeksema, J. T., Liu, Y., Hayashi, K., et al. 2014, *SoPh*, 289, 3483, doi: [10.1007/s11207-014-0516-8](https://doi.org/10.1007/s11207-014-0516-8)
- Jiang, C.-q., & Mei, Z. 2019, *ChA&A*, 43, 252, doi: [10.1016/j.chinastron.2019.04.009](https://doi.org/10.1016/j.chinastron.2019.04.009)
- Jiang, C. Q., & Zhang, M. 2018, *Acta Astronomica Sinica*, 59, 39
- Kosugi, T., Matsuzaki, K., Sakao, T., et al. 2007, *SoPh*, 243, 3, doi: [10.1007/s11207-007-9014-6](https://doi.org/10.1007/s11207-007-9014-6)
- Lites, B. W., & Ichimoto, K. 2013, *SoPh*, 283, 601, doi: [10.1007/s11207-012-0205-4](https://doi.org/10.1007/s11207-012-0205-4)
- Liu, S., Su, J. T., Zhang, H. Q., et al. 2013, *PASA*, 30, e005, doi: [10.1017/pasa.2012.005](https://doi.org/10.1017/pasa.2012.005)
- Low, B. C. 1985, in *Measurements of Solar Vector Magnetic Fields*, ed. M. J. Hagyard, 49–65
- Low, B. C. 1992, *ApJ*, 399, 300, doi: [10.1086/171925](https://doi.org/10.1086/171925)
- Low, B. C., & Lou, Y. Q. 1990, *ApJ*, 352, 343, doi: [10.1086/168541](https://doi.org/10.1086/168541)
- Metcalf, T. R., Jiao, L., McClymont, A. N., Canfield, R. C., & Uitenbroek, H. 1995, *ApJ*, 439, 474, doi: [10.1086/175188](https://doi.org/10.1086/175188)
- Metcalf, T. R., Leka, K. D., Barnes, G., et al. 2006, *SoPh*, 237, 267, doi: [10.1007/s11207-006-0170-x](https://doi.org/10.1007/s11207-006-0170-x)
- Moon, Y. J., Choe, G. S., Yun, H. S., Park, Y. D., & Mickey, D. L. 2002, *ApJ*, 568, 422, doi: [10.1086/338891](https://doi.org/10.1086/338891)
- Scherrer, P. H., Schou, J., Bush, R. I., et al. 2012, *SoPh*, 275, 207, doi: [10.1007/s11207-011-9834-2](https://doi.org/10.1007/s11207-011-9834-2)
- Tiwari, S. K. 2012, *ApJ*, 744, 65, doi: [10.1088/0004-637X/744/1/65](https://doi.org/10.1088/0004-637X/744/1/65)
- Toriumi, S., & Takasao, S. 2017, *ApJ*, 850, 39, doi: [10.3847/1538-4357/aa95c2](https://doi.org/10.3847/1538-4357/aa95c2)
- Toriumi, S., Takasao, S., Cheung, M. C. M., et al. 2020, *ApJ*, 890, 103, doi: [10.3847/1538-4357/ab6b1f](https://doi.org/10.3847/1538-4357/ab6b1f)
- Wiegmann, T., & Inhester, B. 2010, *A&A*, 516, A107, doi: [10.1051/0004-6361/201014391](https://doi.org/10.1051/0004-6361/201014391)
- Wiegmann, T., Inhester, B., & Sakurai, T. 2006, *SoPh*, 233, 215, doi: [10.1007/s11207-006-2092-z](https://doi.org/10.1007/s11207-006-2092-z)

Wiegmann, T., & Sakurai, T. 2021, Living

Reviews in Solar Physics, 18, 1,

doi: [10.1007/s41116-020-00027-4](https://doi.org/10.1007/s41116-020-00027-4)

Wiegmann, T., Thalmann, J. K., Inhester, B.,
et al. 2012, SoPh, 281, 37,

doi: [10.1007/s11207-012-9966-z](https://doi.org/10.1007/s11207-012-9966-z)

Zhang, M., & Low, B. C. 2005, ARA&A, 43, 103,

doi: [10.1146/annurev.astro.43.072103.150602](https://doi.org/10.1146/annurev.astro.43.072103.150602)

Zhang, X. M., Zhang, M., & Su, J. T. 2017, ApJ,
834, 80, doi: [10.3847/1538-4357/834/1/80](https://doi.org/10.3847/1538-4357/834/1/80)

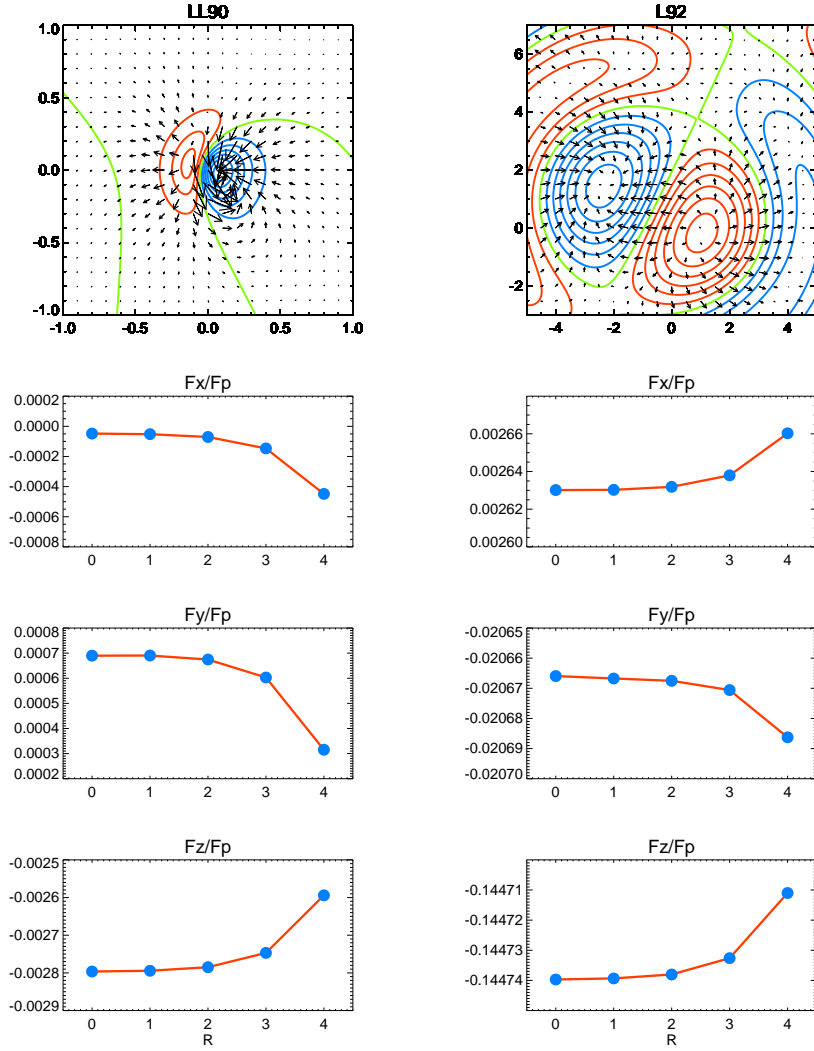


Figure 1. From top to bottom panels present the magnetogram, F_x/F_p , F_y/F_p and F_z/F_p values for the analytical force-free magnetic field (left panels) and non-force-free magnetic field (right panels). The x-axis in the bottom six panels is the resolution-index R , with $R = 0$ of the original spatial resolution. See text for more details.

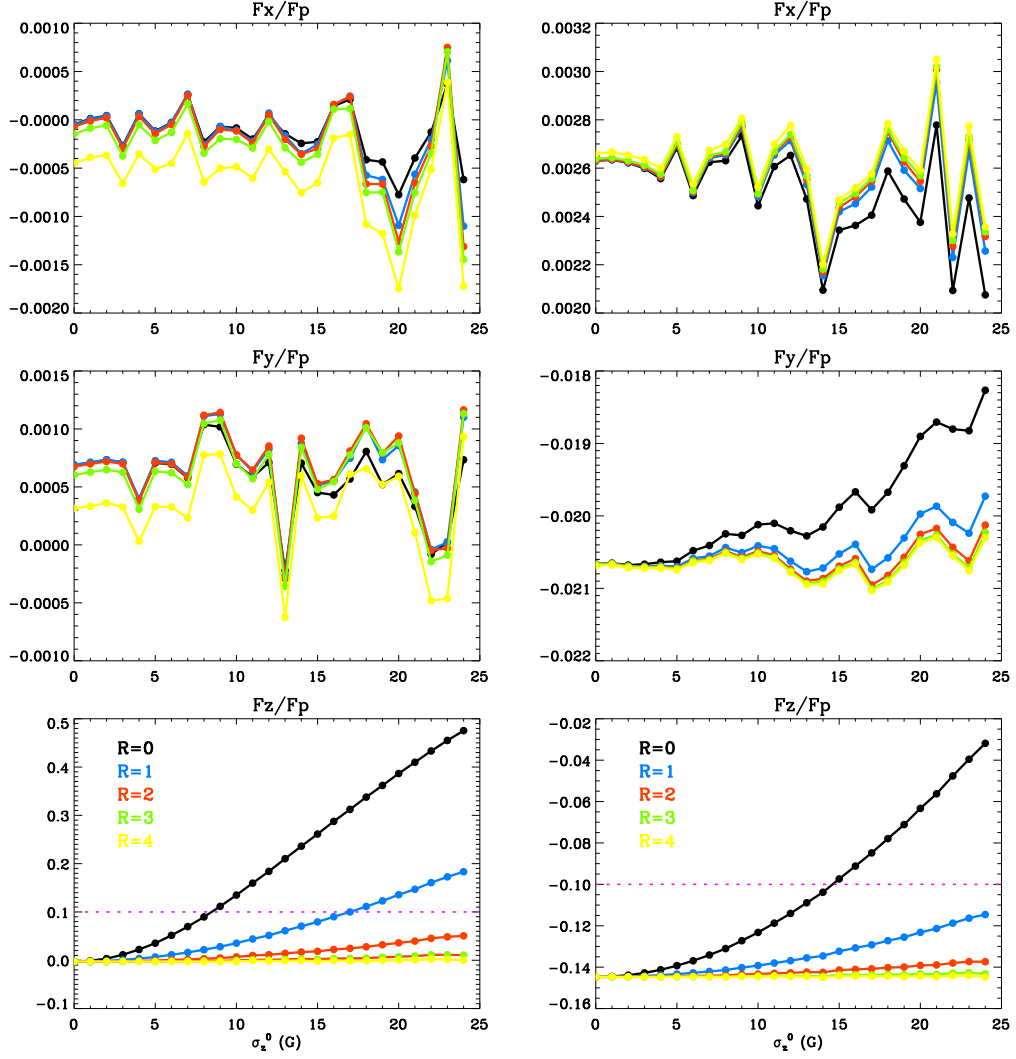


Figure 2. From top to bottom panels present the F_x/F_p , F_y/F_p and F_z/F_p values for the analytical force-free magnetic field (left panels) and non-force-free magnetic field (right panels). The x-axis is the noise level in the vertical field (σ_z^0). Values obtained from magnetograms with different spatial resolutions are presented in different colors, black for R=0, blue for R=1, red for R=2, green for R=3 and yellow for R=4. See text for more details.

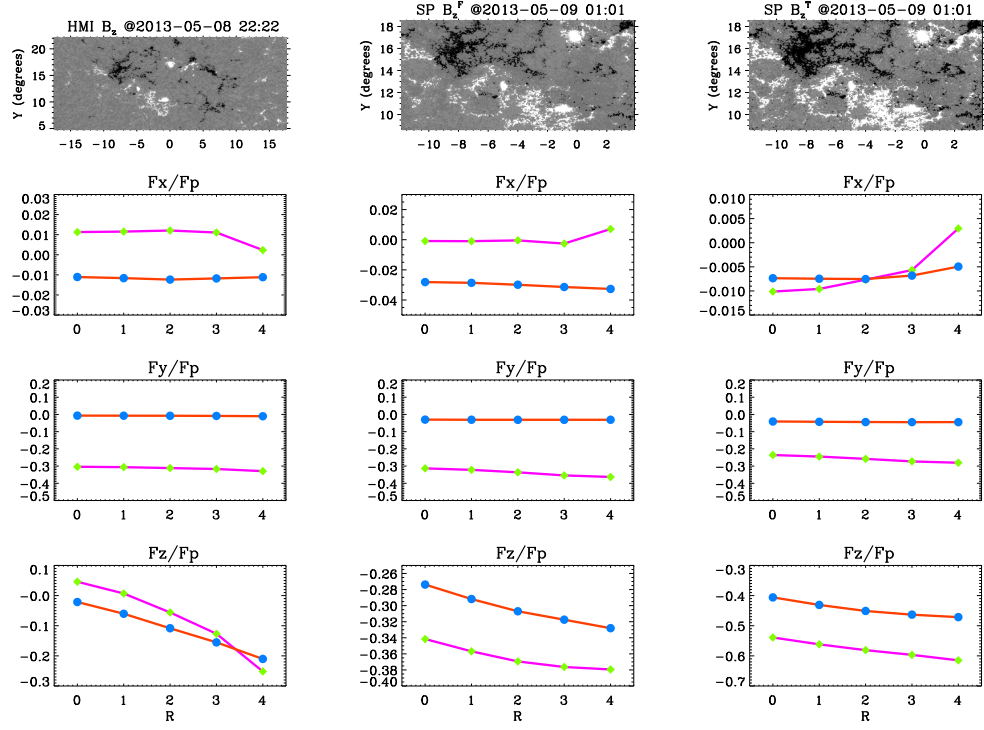


Figure 3. From top to bottom panels present the magnetogram of NOAA 11739, F_x/F_p , F_y/F_p and F_z/F_p values. Left panels are of the HMI/SDO data, middle panels are of the SP/Hinode “flux density” data and right panels are of the SP/Hinode “true field strength” data. The x-axis in the bottom nine panels is the resolution-index R . The green filled-diamond points are of the NOAA 11739. The blue filled-circle points present the corresponding mean values in each sample (those also shown in Figures 4 - 6). See text for more details.

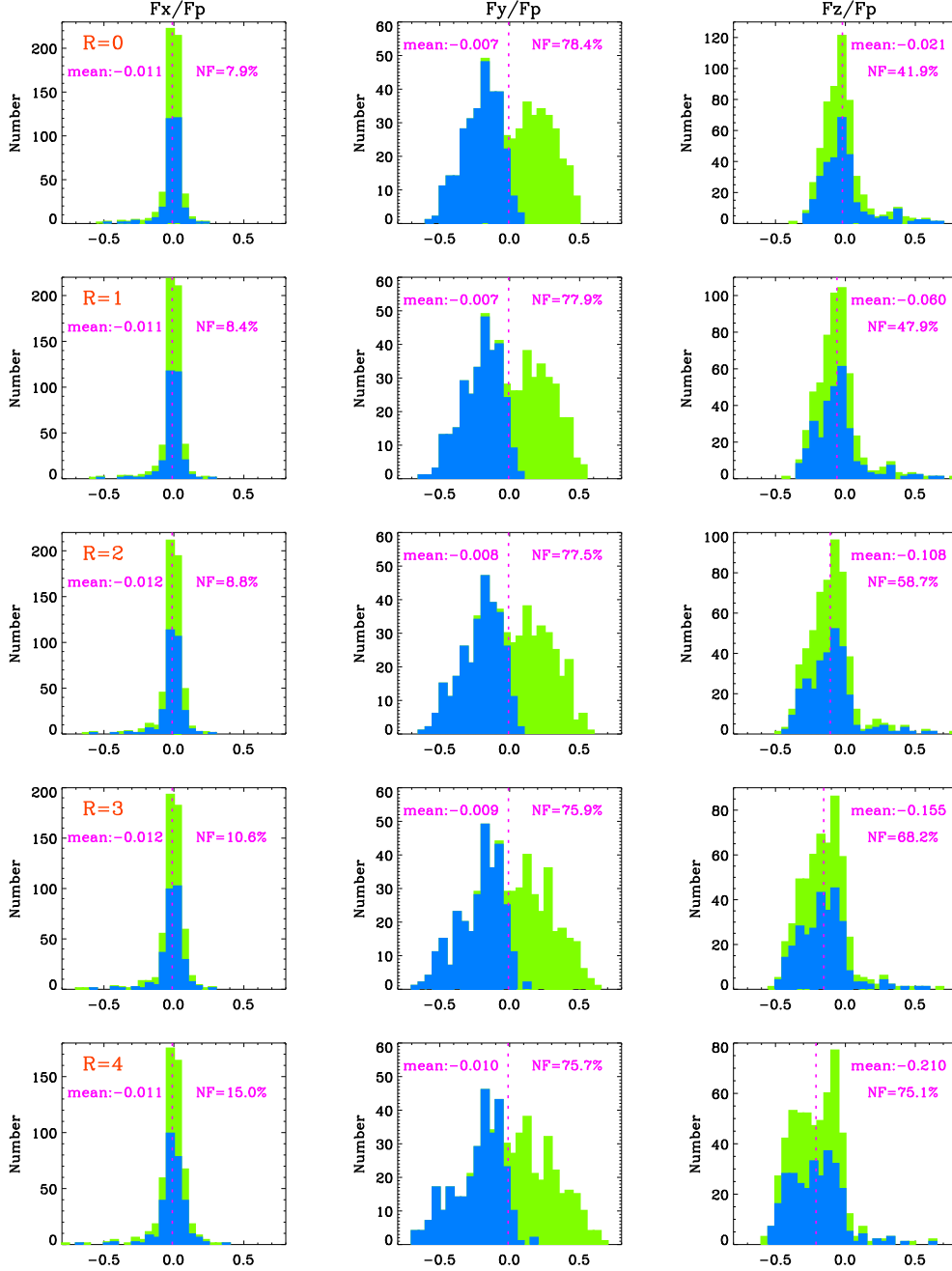


Figure 4. The histograms of the F_x/F_p (left panels), F_y/F_p (middle panels) and F_z/F_p (right panels) values of the 547 HMI/SDO magnetograms. From top to bottom panels are of the $R = 0, 1, 2, 3, 4$ magnetograms respectively. Blue shows the portion of active regions in the northern hemisphere and green the portion of active regions in the southern hemisphere. Mean value and the NF (Non-force-free percentage) value are also listed in each panel. Vertical purple line in each panel shows where the mean value lies.

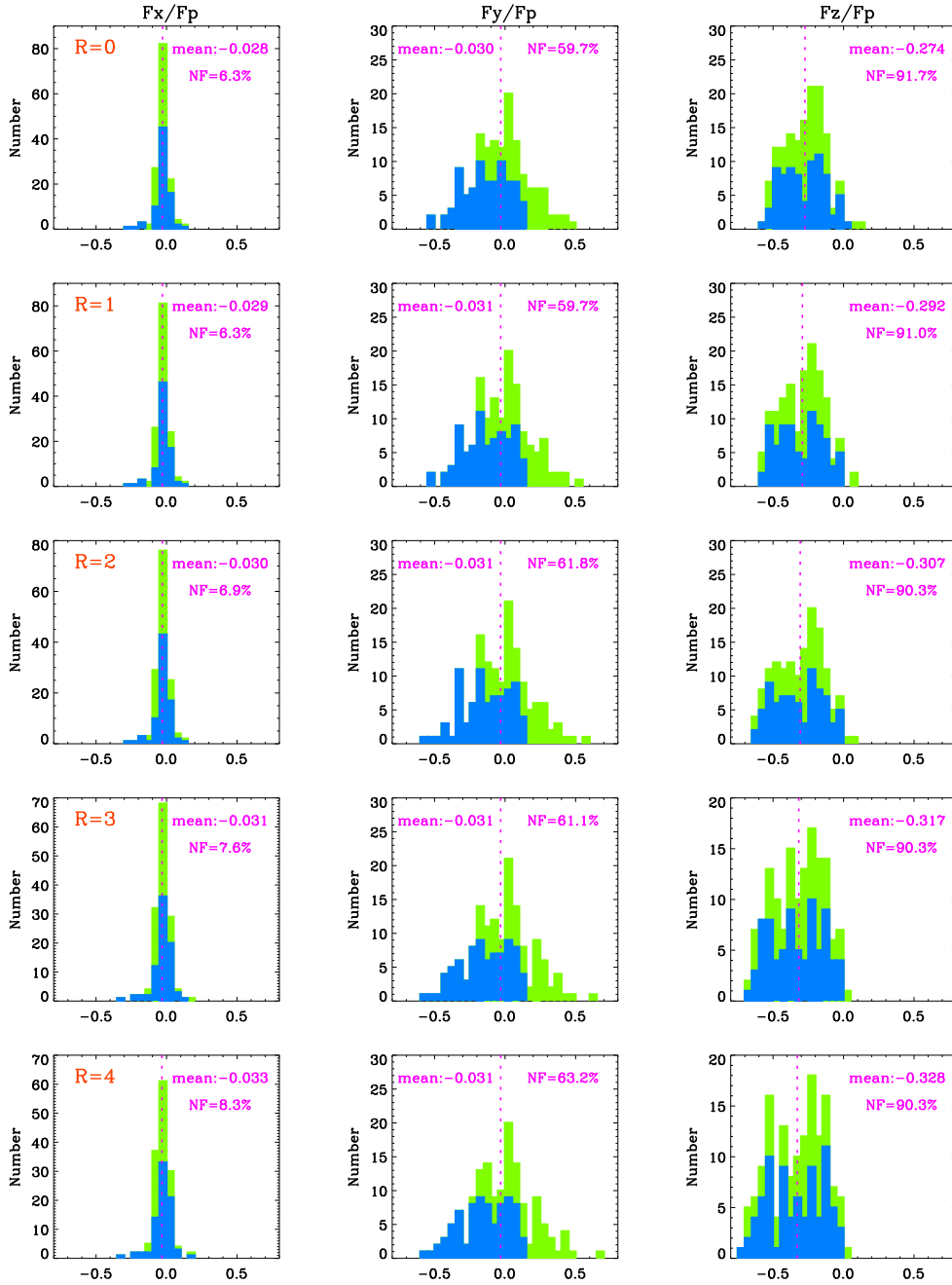


Figure 5. Same as Figure 4 but for the sample of the 144 SP/Hinode “flux density” magnetograms.

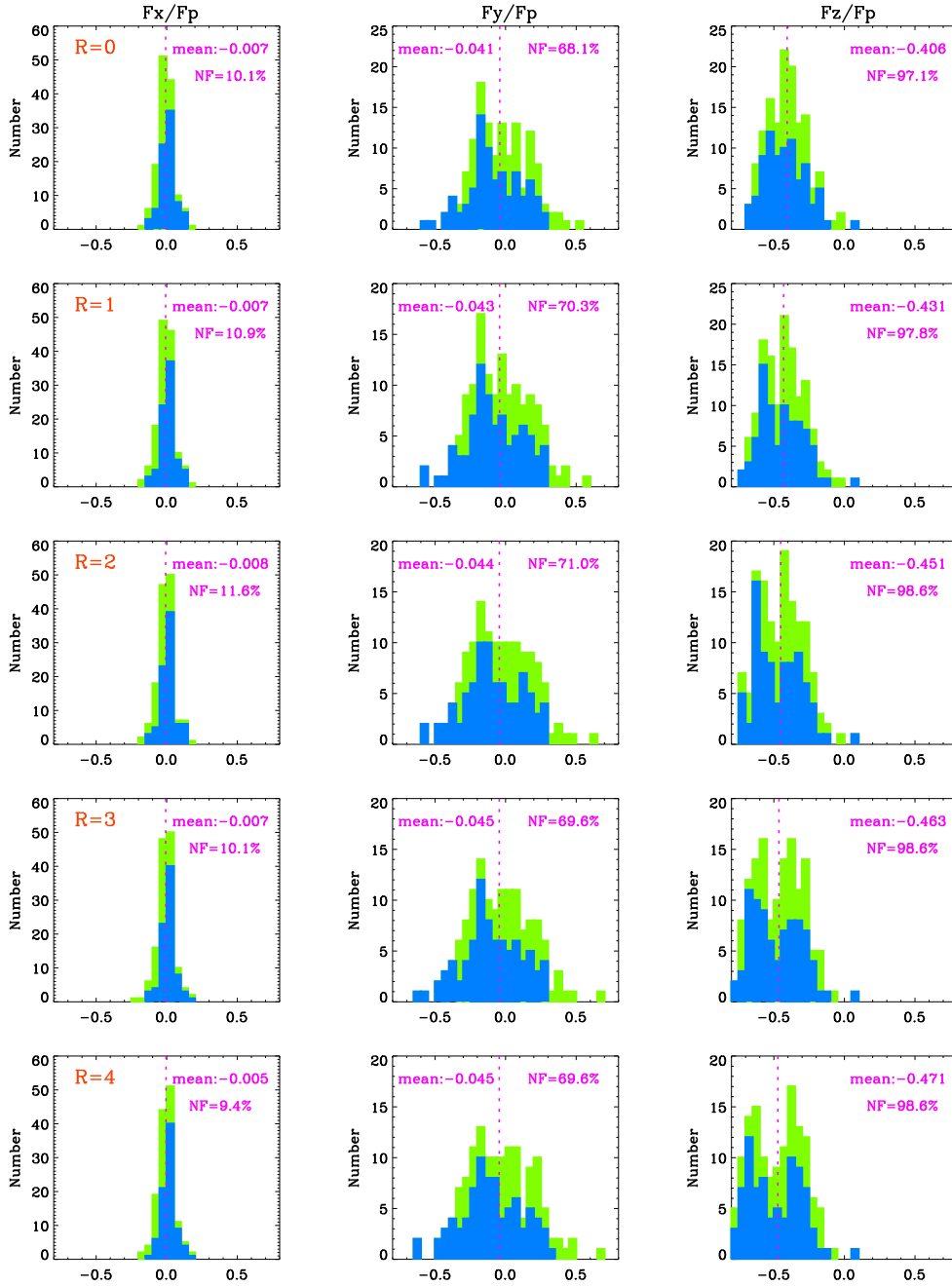


Figure 6. Same as Figure 4 but for the sample of the 138 SP/Hinode “true field strength” magnetograms.